Journal of Applied Fluid Mechanics, Vol. 11, No. 4, pp. 1021-1031, 2018.
Available online at www.jafmonline.net, ISSN 1735-3572, EISSN 1735-3645.
DOI: MDIP .27603

Transition from Steady to Oscillatory Flow Natural Convection of Low-Pr Fluids in 3D Bridgman Configuration for Crystal Growth

A. Atia, B. Ghernaout and S. Bouabdallah†

LME, Laboratory of Mechanics, University of Laghouat, Laghouat 03000, Algeria

†*Corresponding Author Email: fibonsaid@gmail.com*

(Received January 17, 2017; accepted January 22, 2018)

ABSTRACT

A numerical study of the transition from steady to oscillatory flow natural convection of low- Prandtl number fluids inside the 3D Bridgman configuration has been carried out. The three-dimensional Navier-Stokes and energy equations, with the Boussinesq approximation have been discretized by means of a finite volume procedure which employs a second order accurate central difference scheme to treat diffusive and convective fluxes. In natural convection, the buoyancy force is only driving the flow and its intensity can be move a harmful effect on the crystal growth, such as the striation. Naturally, the steady state flow is obtained for low Rayleigh number and shows a great dependence between the Rayleigh number, the flow structure and the heat transfer rate. A low increase in the Rayleigh number we guide to determine the critical point in which the 3D flow became oscillatory. This regime appears by a sinusoidal signal in the time and developed in each period of time.

Keywords: 3D Natural convection, Steady-oscillatory flow, Low-Pr fluid, Numerical study.

NOMENCLATURE

g	gravitational acceleration, m. s^{-2}	β	thermal expansion coefficient, K^{-1}
L	length of the enclosure, m	θ	dimensionless temperature
Nu_{avr}	average Nusselt number	ρ	density of the fluid, kg. m^{-3}
P	dimensionless pressure	τ	dimensionless time
Pr	Prandtl number	υ	kinematic viscosity, $m^2.s^{-1}$
Ra	Rayleigh number	Δ	difference in parameter
T	Temperature, K	Subscripts	
U	dimensionless horizontal velocity	c	Cold
V	dimensionless vertical velocity	cr	critical value
W	dimensionless transversal velocity	h	hot
X,Y,Z	dimensionless Cartesian coordinates	m	melting
α	thermal diffusivity, $m^2.s^{-1}$	max	maximum value

1. INTRODUCTION

The electronics industry requires a strong demand for semiconductor materials and severe requirement of their quality. These crystals are produced from molten baths using various crystal growth techniques (Bridgman, float zone, Czochralski ...). A sufficiently high gradient of temperature in the melt characterizing the crystal growth by horizontal Bridgman technique (HB). These thermal gradients are the source of the gravitational forces which generate substantial convective motion within the fluid.

These convective motion constituents an important energy transfer mode that can speed up the process and affect significantly the quality of the crystal formed (Semma *et al.* 2004). It is recognized that the convection in the liquid is laminar and stable with respect to small numbers of Rayleigh. However, natural convection can become oscillatory and periodic in time from some value, called critical value, for which the behavior of the flow suddenly becomes qualitatively different from past behavior. This critical value is very important

where it helps the experimenters and industrial of crystallography for the manufacture of semiconductors in good conditions.

Several experiments were make for a pure molten Gallium in enclosure exposed to the horizontal temperature gradient shows the flow oscillation (Hurel *et al*. 1974). Also, for the cavity exposed to the differentially heated vertical walls. For a low gradient temperature, the flow manifests unicellular, but for a sufficient temperature gradient the flow becomes oscillatory when the critical temperature difference (ΔT_{cr}) achieved. So, the unicellular flow bifurcated. Also, Hart (1983) published a report of measurements on the oscillatory regime, critical Grashof number, frequency and wavelength for a wide aspect ratio of cell filled with mercury. He obtain a good agreement with an analytical model derived for infinitely extended layers, and confirms the instability flow in the same axis of temperature gradient.

Some valuables information's were obtained by numerical simulation of oscillatory regimes in low-Pr fluids. Such as the existence of the oscillatory regimes in 2D rectangular cavities was showed by Crochet *et al*. (1983, 1987), Roux *et al*. (1985) and Ben Hadid and Roux (1987). In two dimensional models with 4×1 box the threshold value of Gr for the onset of oscillation and their corresponding frequency (Roux, 1990) agreed to the value obtained by Winters (1888), and compared with the results of Hurle *et al.* (1974), and Hung and Andereck (1990). Although they are ignored these simulations are sufficient to explain the oscillatory regime in 3D models close to reality.

Gadoin *et al.* (2001) presented a general methodology for study the flow instability of natural convection in complex cavities. The principle of their methodology has been exposed with the preliminary results. Their methodology can be applied to understanding the transition to unstable and chaotic regimes for internal flows. A comparison between numerical and experimental results for the onset of 3D oscillatory flow of molten Gallium in rectangular cavity heated laterally was reported by Hof *et al*. (2004). They found that the transition threshold takes place where there is a supercritical Hopf bifurcation.

The dependence of critical Grashof number and oscillation frequency with aspect ratio of the rectangular cavity ($1 \leq Ar \leq 10$), and for different cases of the Prandtl numbers was studied by Gelfgat and Tanzawa (1994). Diagrams of stability which show that this dependence is more complicated and very sensitive to a small change in the control parameter and the convective transfer is not negligible even for low numbers Prandtl. Zhou and Zebib (1992) used a two-dimensional model of the solidification of pure metals in a horizontal rectangular cavity. They examined the influence of oscillatory transition of natural convection and predict the parameters associated with this phenomenon. In particular, the influence of the solidification temperature on the critical Grashof number. They showed that this influence is directly linked with the aspect ratio in the liquid part. The increase in the solidification temperature causes oscillatory convection for high critical Grashof numbers. Bouabdallah *et al.* (2011) used the finite volume method to study flow field in a 3D cavity filled with molten Gallium under action of the magnetic field. They found a steady state flow when the value of critical Grashof number equal to $Gr = 3\times10^5$, and unsteady oscillatory flow when the Gr reaches 3.375×10^5. They found also that this critical value increase in presence of magnetic field.

Ho *et al.* (2001) investigate the natural-convection-dominated melting of ice inside a rectangular enclosure. They show in the water region during melting process the appearance of the temporal oscillatory convection flow and temperature. Afrid and Zebib (1990) simulated a 3D convection flow with a hypothesis of symmetry according to the 3rd dimension which does not confuse with the experimental reality (see Pratte and Hart (1990)). Recently, Atia *et al*. (2016) studied the onset of oscillatory mixed convection of the Silicon melt ($Pr = 0.011$) in Czochralski configuration. They obtained the transition to oscillatory flow for $Re_{cr} = 3010$, and this value increase with increasing the magnetic field intensity.

The purpose of the present work is to answers on some questions and comments received from the reviewers of our published works (Bouabdallah *et al*. 2011; Atia *et al*. 2016). So, the transition point from the steady to oscillatory state flow convection in low-Pr fluid is the highest subject of this study. Also, to see what happening character of the oscillatory natural convection in the time and flow structure. So, the two cases: steady state natural convection and the oscillatory natural convection flow of low-Pr fluids, time-dependent flow and it development on hydrodynamics and thermal field were presented.

2. PROBLEM DESCRIPTION AND MATHEMATICAL FORMULATION

The problem under consideration, shown in Fig. 1, is a cubical enclosure similar to that used in horizontal Bridgman technique (HB) for crystal growth. This enclosure filled by low-Pr fluid. The vertical walls (right and left) are exposed to the temperature gradient, such as $Tc < Tm < Th$, respectively for the cold temperature, melting temperature and hot temperature. The other walls are adiabatic. We take the all thermal, physical and electrical proprieties of low-Pr fluid from the Metals Handbook (1990).

By neglecting the viscous dissipation, Joule heating, and using the parameters $L, \upsilon/L$, L^2/υ, $\rho_0(\upsilon/L)^2$ and $(T_h\text{-}T_c)$ (Zhao *et al*. 2016) as typical scales for lengths, velocities, time, pressure and temperature, respectively. The dimensionless governing equations for an incompressible flow, in which we assume a Newtonian fluid and use the Boussinesq approximation, are:

Continuity equation

$$\frac{\partial U}{\partial X}+\frac{\partial V}{\partial Y}+\frac{\partial W}{\partial Z}=0 \quad (1)$$

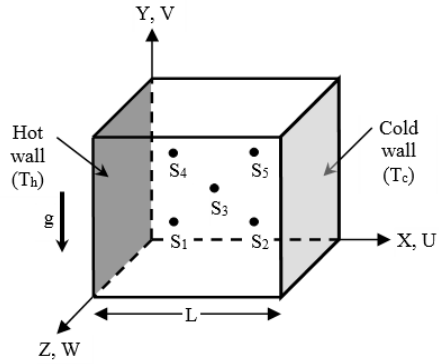

Fig. 1. Geometry of the problem (S_1-S_5 are the monitoring points)

X-momentum equation

$$\frac{\partial U}{\partial \tau}+\frac{\partial (UU)}{\partial X}+\frac{\partial (VU)}{\partial Y}+\frac{\partial (WU)}{\partial Z}= -\frac{\partial P}{\partial X}+\left(\frac{\partial^2 U}{\partial X^2}+\frac{\partial^2 U}{\partial Y^2}+\frac{\partial^2 U}{\partial Z^2}\right) \quad (2)$$

Y-momentum equation

$$\frac{\partial V}{\partial \tau}+\frac{\partial (UV)}{\partial X}+\frac{\partial (VV)}{\partial Y}+\frac{\partial (WV)}{\partial Z}= -\frac{\partial P}{\partial Y}+\left(\frac{\partial^2 V}{\partial X^2}+\frac{\partial^2 V}{\partial Y^2}+\frac{\partial^2 V}{\partial Z^2}\right)+\mathrm{Pr.Ra.}\theta \quad (3)$$

Z-momentum equation

$$\frac{\partial W}{\partial \tau}+\frac{\partial (UW)}{\partial X}+\frac{\partial (VW)}{\partial Y}+\frac{\partial (WW)}{\partial Z}= -\frac{\partial P}{\partial Z}+\left(\frac{\partial^2 W}{\partial X^2}+\frac{\partial^2 W}{\partial Y^2}+\frac{\partial^2 W}{\partial Z^2}\right) \quad (4)$$

Energy equation

$$\frac{\partial \theta}{\partial \tau}+\frac{\partial (U\theta)}{\partial X}+\frac{\partial (V\theta)}{\partial Y}+\frac{\partial (W\theta)}{\partial Z}= \frac{1}{\mathrm{Pr}}\left[\frac{\partial^2 \theta}{\partial X^2}+\frac{\partial^2 \theta}{\partial Y^2}+\frac{\partial^2 \theta}{\partial Z^2}\right] \quad (5)$$

Where U, V and W are dimensionless velocity components in the X, Y, and Z directions. $\theta = T-T_c/T_h-T_c$, $\mathrm{Pr}=\upsilon/\alpha$, $\mathrm{Ra}=g\beta\Delta TL^3/\upsilon\alpha$, represents the dimensionless temperature, Prandtl number and Rayleigh number, respectively. $g, \beta, \upsilon, \alpha$ are the gravitational acceleration, thermal expansion coefficient, kinematic viscosity of the fluid, and thermal diffusivity, respectively. The above equations have been associated to the following conditions:

At $\tau = 0$: $U = V = W = 0$, $\theta = 0$ (6a)

For $\tau > 0$:

At $X = 0$, $0 \le Y \le 1$ and $0 \le Z \le 1$: $U = V = W = 0$, $\theta = 1$ (Hot right wall) (6b)

At $X = 1$, $0 \le Y \le 1$ and $0 \le Z \le 1$: $U = V = W = 0$, $\theta = 0$ (Cold left wall) (6c)

At $Y = 0$, $0 \le X \le 1$ and $0 \le Z \le 1$: $U = V = W = 0$,

$\frac{\partial \theta}{\partial Y} = 0$ (Adiabatic bottom wall) (6d)

At $Y = 1$, $0 \le X \le 1$ and $0 \le Z \le 1$: $U = V = W = 0$,

$\frac{\partial \theta}{\partial Y} = 0$ (Adiabatic top wall) (6e)

At $Z = 0$, $0 \le X \le 1$ and $0 \le Y \le 1$: $U = V = W = 0$,

$\frac{\partial \theta}{\partial Z} = 0$ (Adiabatic back wall) (6f)

At $Z = 1$, $0 \le X \le 1$ and $0 \le Y \le 1$: $U = V = W = 0$,

$\frac{\partial \theta}{\partial Z} = 0$ (Adiabatic front wall) (6g)

3. NUMERICAL METHOD

Governing equations (Eqs. 1-5) with the associated initial and boundary conditions (Eqs. 6a- g) were solved using a finite-volume method. The velocity components (U, V, and W) are stored at the staggered locations, and the scalars quantities (P and θ) are stored at the center of these volumes. The numerical procedure called SIMPLER is used to handle the pressure-velocity coupling. The second-order accurate central difference scheme is used to discretize the convection and diffusion terms. Temporal discretization is first order accurate and fully implicit. Finally, the discretized algebraic equations are solved by the line-by-line tridiagonal matrix algorithm (TDMA). Convergence at a given time step is declared when the maximum relative change between two consecutive iteration levels fell below than 10^{-4}, for U, V, W and θ. At this stage, the steady state solution is obtained. A parallel test was made to guarantee that the energy balance between the hot and cold walls is less than a prescribed accuracy value, i.e., 0.2%.

3. 1. Effect of Mesh Size

Various mesh sizes are selected to ensure the mesh independency study, 32^3 (32768 nodes), 42^3 (74088 nodes), 52^3 (140608 nodes), 62^3 (238328 nodes), 72^3 (373248 nodes), and 82^3 (551368 nodes). Results are achieved for molten Gallium with $\mathrm{Ra} = 5 \times 10^4$. In Figs. 2a-c, we have presented the profiles of the maximum dimensionless velocity components (U_{max}, V_{max}), and the average Nusselt number (Nu_{avr}) for various mesh sizes. It is found that the variation of the velocity components and Nusselt number remains almost constant from the mesh size 62^3. According to Figs. 2a-c, and to arrange the choice between calculation time and accuracy of calculations, the 62^3 grid is found suitable. Calculations were carried out on a Work Station (CPU Core 2 Quad Q9625, 3.00 GHZ-12 Mo. L2); the average computing time for a typical case was approximately 7 hours.

3. 2. Validation/Comparison of the Results

Two cases are examined to validate the numerical

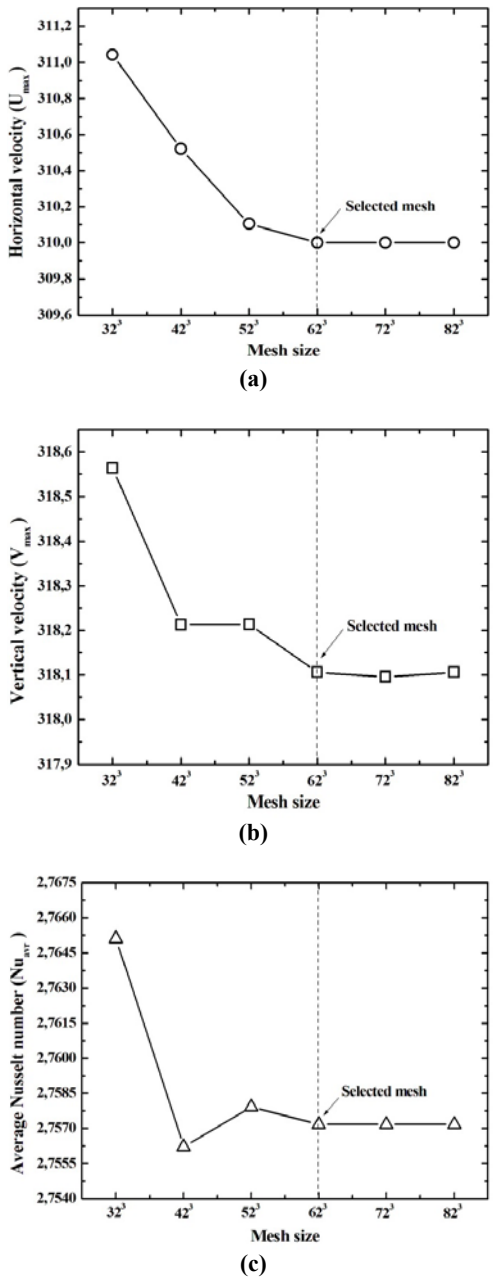

Fig. 2. Effect of the mesh sizes on the profiles of velocity components (a, b), and the average Nusselt number (c), for Ra = 5 × 10^4.

simulation by using the computer code. Achieved results are compared with the existing experimental and numerical results in literature. Firstly, the comparison is made with experimental work of Krane and Jessee (1983). In Figs. 3a-b, we have presented the comparison of the vertical velocity component (V) and dimensionless temperature distribution (θ) in the middle of the enclosure for Ra = 1.89×10^5 and Pr = 0.71. Secondly the comparison is made with numerical work of Fusegi *et al*. (1991). The iso-surfaces of the temperature in 3D enclosure for two Rayleigh numbers Ra = 10^4 and 10^6 are presented in Fig. 3c, where the work of Fusegi *et al*. (1991) at the left. From these figures, a good agreement is observed with the numerical and experimental results.

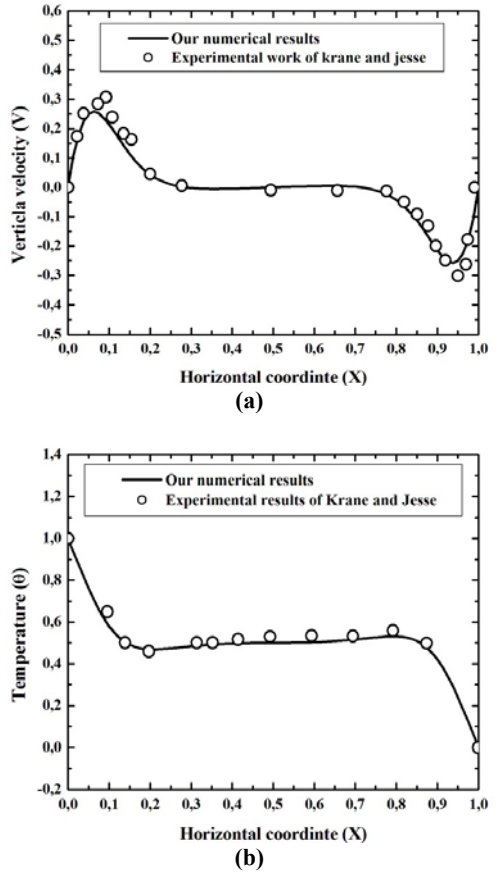

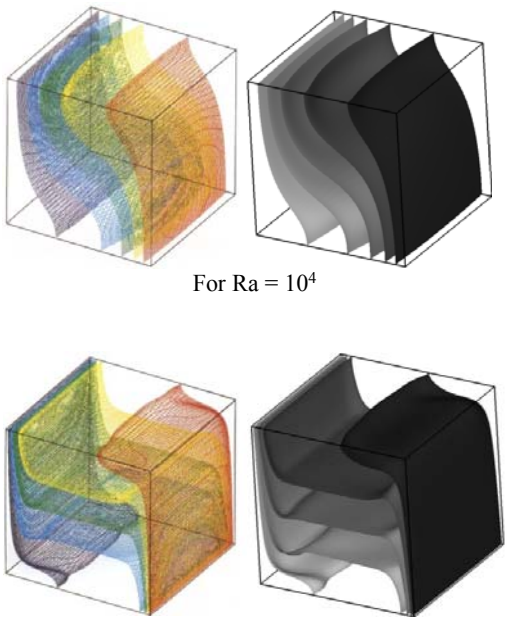

Fig. 3. Comparison of our results with experimental data of Krane and Jessee (1983) (a-b), and numerical simulation of Fusegi *et al.* (1991); iso-surfaces of the temperature in 3D enclosure, for two values of Rayleigh number (10^4 and 10^6).

4. RESULTS AND DISCUSSION

We present the results of the transition from steady to oscillatory flow natural convection of low-Pr fluids which is contained in a cubical enclosure. The natural convection can be controlled by the Rayleigh number. So, for a low value, the steady-state is displayed and when the Rayleigh number is increased, the oscillatory flow starting with a critical value.

Some measurement probes (points) in computational domain (S_1, S_2, S_3, S_4 and S_5) were shown schematically in Fig. 1. These points are located in the main areas of the enclosure: the heart, near vertical walls and near horizontal walls to store the temporal evolution of the velocity and temperature in order to detect the physical instabilities. The coordinates of these points are presented in Table 1. All results presented herein are given in dimensionless form.

Table 1 Dimensionless coordinates of the monitoring points S_1, S_2, S_3, S_4 and S_5.

Monitoring points	S_1	S_2	S_3	S_4	S_5
X	0.2	0.8	0.5	0.2	0.8
Y	0.2	0.2	0.5	0.8	0.8
Z	0.5	0.5	0.5	0.5	0.5

4.1. Steady State of Natural Convection Flow

In this section, we study the flow field of 3D natural convection in steady state of the molten Gallium (Pr = 0.025). For this, we have plotted the iso-surfaces of the temperature, and the path lines of some fluid particles for various values of the Rayleigh number $Ra \leq 2 \times 10^5$ (low values, steady state flow convection). Figure 4, presents the temporal evolution of the flow parameters (U, V, W and θ) at different points. We can see that the steady state flow extends to $Ra = 2 \times 10^5$. These curves are composed of two parts: oscillatory part due to initial conditions that are taken at the beginning of the calculation, and a portion which tends to an asymptotic limit and stabilizes with time. In this case, we can conclude that the flow in the enclosure is steady. Note that the travel time and the selected initial conditions have an influence on the time to alleviation of asymptotic limit.

Figure 5 presents the iso-surfaces of the temperature and path lines of some fluid particles in the 3D enclosure for various values of the Rayleigh number (steady state flow). For $Ra = 10^3$ (Fig. 5a), we can see that the iso-surfaces of the temperature are parallel to the vertical walls (hot and cold). This indicates that, for low values of Rayleigh number, the heat transfer is done by conduction.

For $Ra = 10^4$ (Fig 5b), we see the inclination of iso-surfaces, indicating that the convection heat transfer begins to develop.

From $Ra = 10^5$ (Figs. 5d-e), this iso-surfaces have a

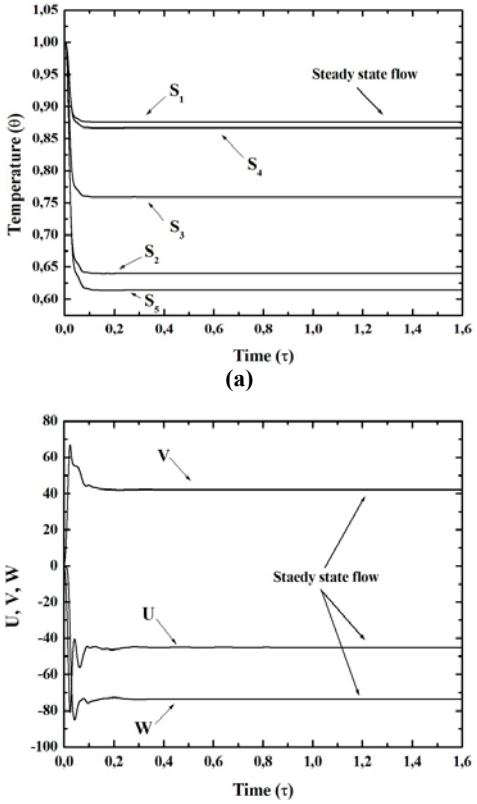

Fig. 4. Temporal evolution of the dimensionless temperature at S_1-S_5 (a) and dimensionless velocity components at S_3 (b), for $Ra = 2 \times 10^5$ (steady state flow)

high curvature in the middle of the enclosure, and become almost vertical near of hot and cold walls. These curves reflect the natural convection in the middle of the enclosure and the conduction heat transfer near the vertical walls and especially in thermal boundary layers that develop near its (hot and cold walls). In addition, with the increase of the Rayleigh number, the intensity of the natural convection is increased. For the path lines of some fluid particles in the enclosure, we see that the flow is regular for low Rayleigh number, but when increasing the Rayleigh number this flow becomes irregular due to dominance of natural convection which accelerates the velocity of fluid particles in the enclosure.

Figures 6a-c, show the dimensionless velocity components for various values of the Rayleigh number. It's clearly seen that the increase of the Rayleigh number causes an increase in the velocity, where the important variation is found for $Ra = 2 \times 10^5$. Also, we notice a negligible change in the transversal velocity compared to the contribution of other velocity components; this reflects that the two-dimensional approximation is sufficient for this problem in steady state. The variation of the average Nusselt number on the hot wall is shown in Fig. 6d. The obtained results show a strong dependence between the Rayleigh number and heat transfer rate, where the convective flow is intense with increasing of the Rayleigh number.

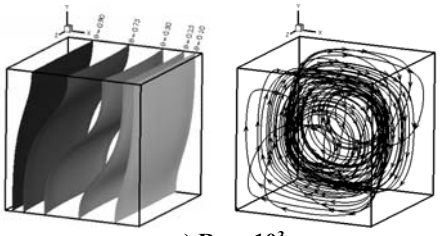

a) Ra = 10^3

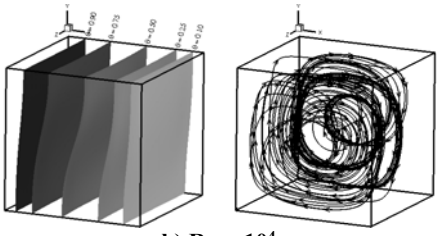

b) Ra = 10^4

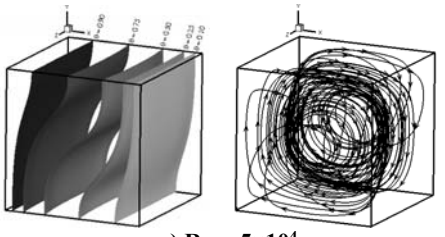

c) Ra = 5×10^4

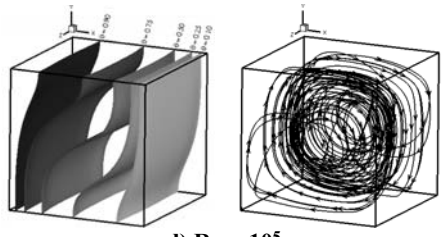

d) Ra = 10^5

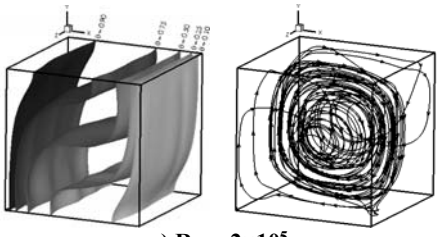

e) Ra = 2×10^5

Fig. 5. Iso-surfaces of the temperature (left) and path lines of some fluid particles (right) in 3D enclosure, for various values of the Rayleigh number (steady state flow).

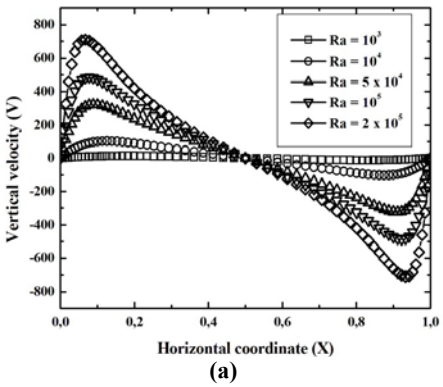

(a)

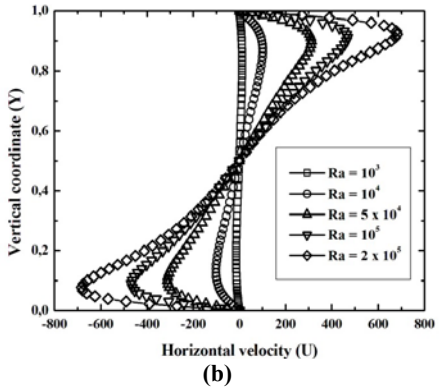

(b)

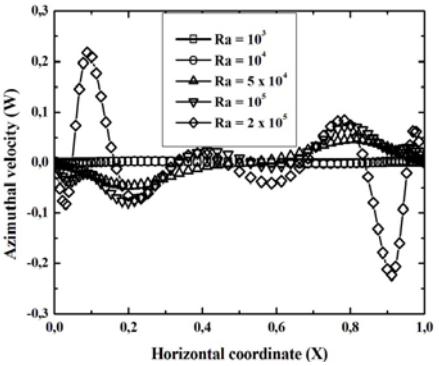

(c)

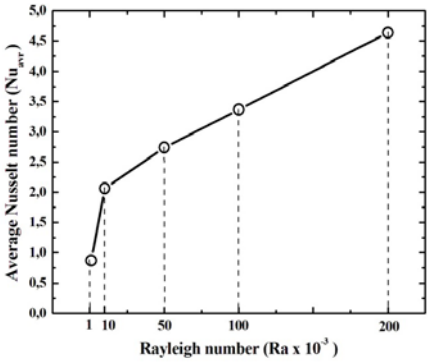

(d)

Fig. 6. Profiles of dimensionless velocity components (a, b, c), and average Nusselt number (d) for various values of the Rayleigh number (steady state flow)

4.2 Oscillatory State of Natural Convection Flow

In the following, we study the transition to oscillatory flow convection for the molten Gallium (Pr = 0.025). The unsteady flow rests on the detection of the critical value of Rayleigh number Ra_{cr}, in which the flow becomes oscillatory and periodic in the time. So, we select a suitable dimensionless step time $\Delta\tau = 10^{-5}$. An increase of Rayleigh from the steady solution achieves the beginning of oscillatory regime. Note that the steady state has been obtained until $Ra = 2\times10^5$. Therefore, from this value the flow manifests oscillatory. For $Ra_{cr} = 2.4 \times 10^5$, the flow becomes oscillatory and periodic in time, and to ensure that the flow manifested by sinusoidal oscillations for $\Delta\tau$ is not numerical oscillations (machine borough or calculation errors), we recalculate the obtained

solution with the same flow parameters but for Δτ/2. This method eliminates much the numerical instabilities that may arise during the calculations. If the amplitudes and frequencies of oscillations are the same at all points after reduction of the time, we say that the instability is purely physic (Fig. 7a). Increasing the Rayleigh number after this value (Ra > Ra_{cr}), the flow enters a beyond oscillatory regime where the oscillation will not periodic and leads to a disruption of the flow (Fig. 7b).

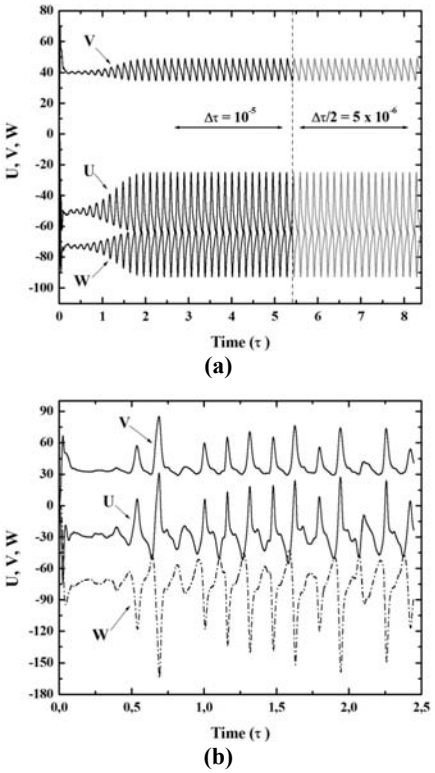

Fig. 7. Variation of the dimensionless vertical velocity components between two time steps for oscillatory flow convection Ra = Ra_{cr} = 2.4 × 10^5 (Pr = 0.025) at S_3 (a), and variation of the dimensionless velocity components for beyond oscillatory flow convection Ra > Ra_{cr} (b).

The oscillatory aspect of the temporal evolution of the flow parameters U, V, W and θ recorded at various points is shown in Figs. 8a-d for Ra_{cr} = 2.4×10^5. The temporal evolution manifests by a sinusoidal signal. So, to show that it presents the physical phenomena we made the dividing of the time steps until no differences observed in the period and amplitude of the signal. We can see that the amplitude of dimensionless temperatures is smallest compared to the velocity component U, V and W, but with identical frequency. The changement in the hydrodynamic and thermal parameters between them constructed the phase portraits. Where the periodic flow plot the closed circles (limit cycle, Stevens *et al.* 1999) and reflect the periodicity of the flow regime (Liu and Tao, 1999).

In Figs. 9a-b, we have plotted the phase portraits at chosen point in enclosure (S_3). These curves for the temporal evolution of temperature/velocity. The curves show that the periodic regime is established. For (Ra > Ra_{cr}) we see the onset of the beyond oscillatory regime (Figs. 9c-d) where the phase

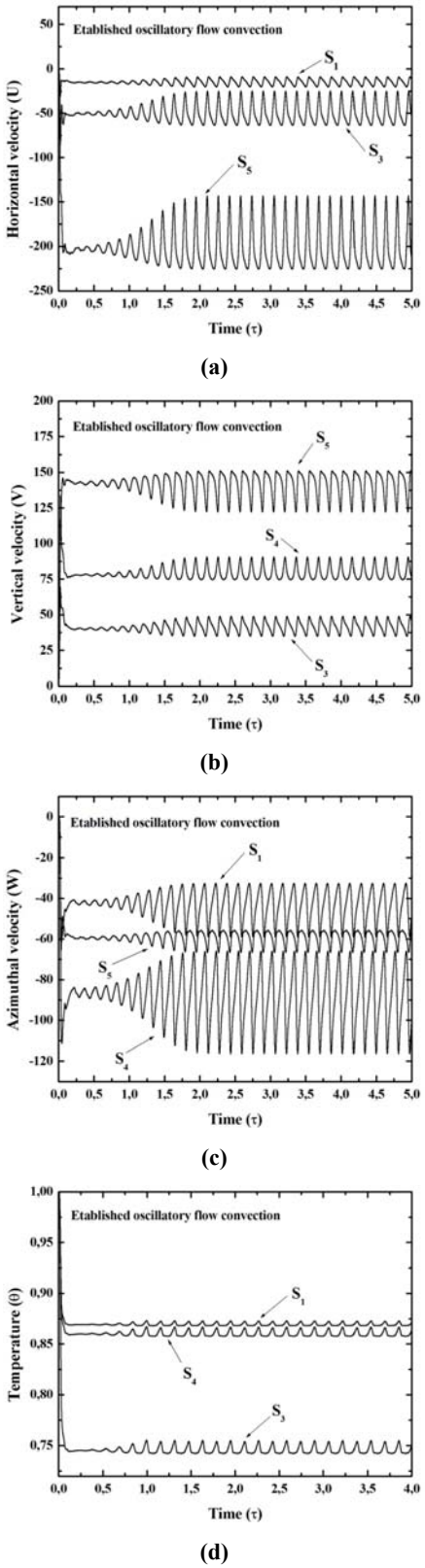

Fig. 8. Time-dependent of dimensionless velocity components (a, b, c) and dimensionless temperature (d) at different monitoring points, for Ra_{cr} = 2.4×10^5 (oscillatory state flow)

portrait has an irregular form (strange attractor), this changement can be explained by the increase of the velocity and temperature of the fluid particles in the enclosure which causes a disruption of the flow.

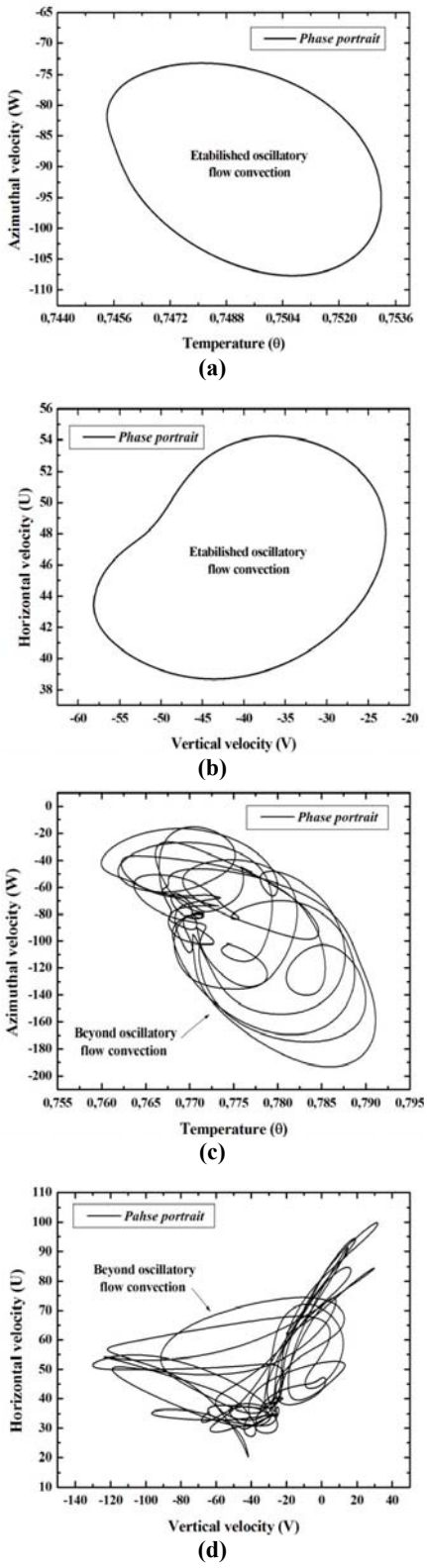

Fig. 9. Phase portraits (W- θ) and (U-V) at S_3. (a, b) oscillatory flow convection for Ra = Ra_{cr}, (c, d) beyond oscillatory flow convection for Ra > Ra_{cr}.

For obtain the energy spectrum of oscillations, we have used the fast Fourier transform (FFT) of a number N of samples of the time variations of various dimensionless parameters. This transform, once multiplied by the half of its conjugate quantity, gives the power spectrum density (PSD) as a function of the oscillation frequencies (Fig. 10), defined by: $F = k / (N \times \Delta\tau)$, where $\Delta\tau$ is the dimensionless time step and k = 1, 2,…, N / 2. Energy has been normalized by N^2. The dimensionless predominant frequencies (The biggest pikes) are considered as those playing the main role in the flow oscillation and therefore the exchange of kinetic and thermal energy. There can exist several others frequencies which are multiples of the dominant one (Atia *et al*. 2016). The multiple-way of the power spectrum present the dominant frequency of the spectrum (Fig. 10a) confirms the periodicity of the flow (oscillatory state flow). On the other hand, if the appearance of these peaks by a non-multiple way to dominate frequency (Fig. 10b) shows that the flow exceeds the oscillatory regime.

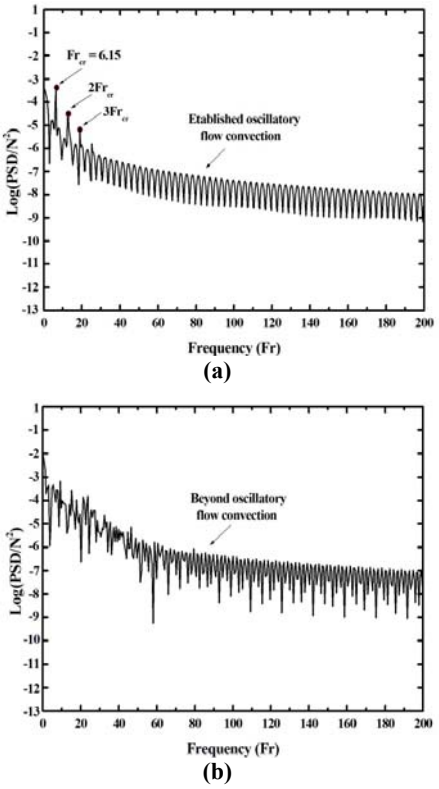

Fig. 10. Power spectrum of the dimensionless radial velocity component, (a) oscillatory flow convection for Ra = Ra_{cr}, (b) beyond oscillatory flow convection for Ra > Ra_{cr}

To give a more detail on the oscillatory flow, it is preferable to present the evolution of the flow parameters over the period of time, for example the azimuthal velocity component W at point S_3 (Fig. 11) at $Ra_{cr} = 2.4 \times 10^5$, with path lines of some fluid particles in selected times: τ_a, τ_b, τ_c, τ_d and τ_e of one period. We note that there is a movement of fluid in clockwise direction from hot to cold wall. We note also that the flow takes a different structure in each

time. At τ_e the flow structure is perfectly similar to the time τ_a, which means that the flow is a periodically.

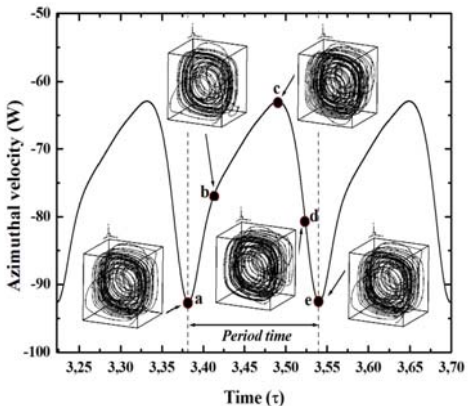

Fig. 11. Time-dependent flow convection with the evolution of path lines of some fluid particles in 3D enclosure at different instants (τ_a, τ_b, τ_c, τ_d, τ_e) constituting one period of time (oscillatory state flow)

4.3. Effect of Prandtl Number

In this part, we see the effect of Prandtl number on the transition from steady to oscillatory flow convection. For this, we added two other fluids Silicon (Pr = 0.011) and Aluminum (Pr = 0.015). Figure 12a shows the time evolution of horizontal velocity (U) for Ra = 2.4×10^5 (corresponds to critical value of the Gallium) and for different Prandtl numbers (Pr = 0.011, 0.015 and 0.025) at S_3. We note that, the variation of Prandtl number has a significant effect on the oscillations. So, that the flow is steady for Pr = 0.011 and 0.015, but it's oscillatory for Pr = 0.025, which means that the increasing of Prandtl number destabilizes the convective flow.

The iso-surfaces of the temperature, iso-surfaces of the horizontal velocity (U = 0.183), and path lines of some fluid particles at dimentionless time τ = 3.0 are presented in Figs 13a-c. For Pr = 0.011 and 0.015 the iso-surfaces of the temperature are parallel to the vertical walls which mean that the heat transfer is purely conductive. For Pr = 0.025 this iso-surfaces appears inclined in the enclosure indicating that the convection is dominated. The iso-surfaces of the horizontal velocity contain two small symmetric iso-surfaces for Pr = 0.011, a little big for Pr = 0.015, and a big nested for Pr = 0.025. The path lines of some fluid particles are well organized in the enclosure, but for Pr = 0.025 the flow destabilized when the heat transfer is purely convective.

The variation of the critical Rayleigh number Ra_{cr} and average Nusselt number Nu_{avr} according to the Prandtl number is summarized in the stability diagram (Fig. 12b). It can see that the increase of the Prandtl number causes the decrease of the critical Rayleigh number, so that the increase in the values of Pr destabilizes the flow in the enclosure, by against, it stabilizes the heat transfer.

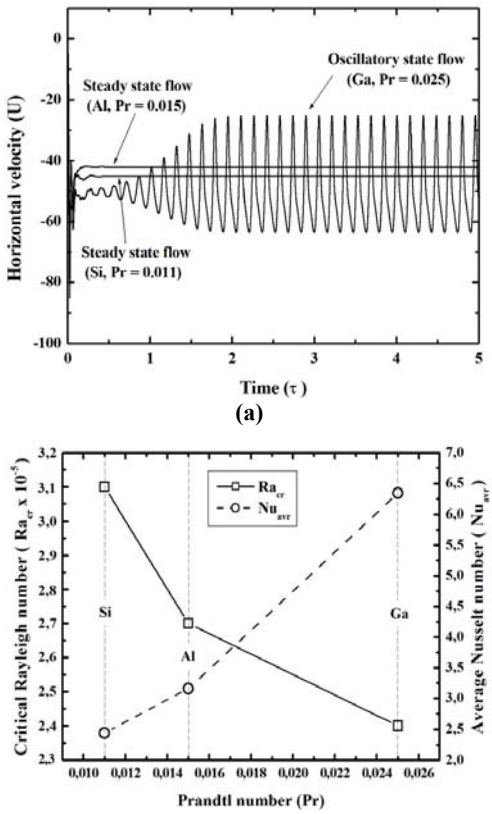

Fig. 12. Time-dependent of dimensionless horizontal velocity component U for different Prandtl numbers (a), and the stability diagrams Ra_{cr}-Pr and Nu_{avr}-Pr (b).

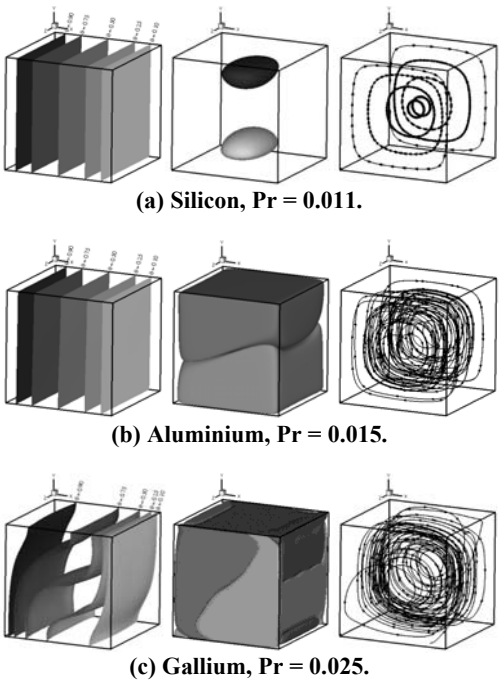

(a) Silicon, Pr = 0.011.

(b) Aluminium, Pr = 0.015.

(c) Gallium, Pr = 0.025.

Fig. 13. Iso-surfaces of the temperature (left), Iso-surfaces of the horizontal velocity (middle), and path lines of some fluid particles (right) at τ = 3.0, for different Prandtl numbers and Ra = 2.4×10^5.

5. CONCLUSION

The transition from steady state to oscillatory flow of three-dimensional natural convection in low-Pr fluids has been numerically presented. The obtained results have been compared with the available data from the literature and good agreement has been found. The obtained results are given from the following points:

- The steady state flow appears at low Rayleigh number, and presents a great dependence between the Rayleigh number, the flow field, and thermal structure.
- A gradually increase in the Rayleigh number permits to determine the critical value of the oscillatory flow convection. This regime appears by the sinusoidal evolution in the time and they developed in each period of time.
- The Prandtl number affect the transition from steady to oscillatory flow convection, where the fast transition is obtained for Pr = 0.025.
- The dependences of the critical Rayleigh number and Nusselt number for various Prandtl numbers were summarized in the stability diagram.

The obtained results may allow researchers and industrialists to see the oscillatory flow of low-Pr fluids in 3D enclosure, in order to improve upon the quality of the semiconductors obtained during the crystal growth by Bridgman technique.

REFERENCES

Afrid, M., Zebib, A. (1990) Oscillatory three-dimensional convection in rectangular cavities and enclosures. *Physics of Fluids* 2, 1318-1327.

Atia, A., Ghernaout, B., Bouabdallah, S., and Bessaïh, R. (2016) Three-dimensional oscillatory mixed convection in a Czochralski silicon melt under the axial magnetic field. *Applied Thermal Engineering* 105, 704-715.

Ben Hadid, H., and Roux, B. (1987) Oscillatory buoyancy-driven convection in horizontal liquid-metal layer, *In Proc., VIth European Symposium on Materials and Fluid Sciences in Microgravity* (ESA SP-256) 477-485.

Bouabdallah, S., Bessaïh, R., Ghernaout, B., Benchatti, A. (2011) Effect of an External Magnetic Field on the 3-D Oscillatory Natural Convection of Molten Gallium During Phase Change. *Numerical Heat Transfer, Part A* 60, 84-105

Crochet, M. J., Geyling, F. T., Van Schaftingen, J.J. (1983) Numerical simulation of the horizontal Bridgman growth of a gallium arsenic crystal. *Journal of Crystal Growth* 65, 166-172.

Crochet, M. J., Geyling, F. T., Van Schaftingen, J.J. (1987) Numerical simulation of the horizontal Bridgman growth. Part 1: two-dimensional flow. *International Journal for Numerical Methods in Fluids* 7, 29-47.

Fusegi, T., Hyun, J. M., Kuwahara, K., Farouk, B. (1991) A numerical study of three dimensional natural convection in a differentially heated cubical enclosure. *International Journal of Heat and Mass Transfer* 34, 1543-1557.

Gadoin, E., Le Quéré, P., Daube, O. (2001) A general methodology for Investigating flow instabilities in complex geometries: application to natural convection in enclosures, *International Journal for Numerical Methods in Fluids* 37, 175-208

Gelfgat, A. Yu., Tansawa, I. (1994) Numerical analysis of oscillatory instability of Buoyancy convection with the Galerkin spectral method. *Numerical Heat Transfer, Part A* 25, 627-648.

Hart, J. E. (1983) A note on the stability of low-Prandtl-number Hadley circulations. *Journal of Fluid Mechanics* 132, 271-281.

Ho C. J., Ho M. J., Yeh, C. T. (2001) Numerical Study of Oscillatory Convection during Melting of Ice in a Rectangular Enclosure. *Numerical Heat Transfer, Part A* 40, 511-530.

Hof, B., Juel, A., Zhao, L., Henry, D., Ben Hadid, H., Mullin, T. (2004) Onset of oscillatory convection in molten Gallium. *Journal of Fluid Mechanics* 515, 391-413.

Hung, M. C., Andereck, C.D. (1990) Subharmonic transitions in convection in a moderately shallow cavity, In Numerical Simulation of Oscillatory Convection in low-Pr Fluids. *Notes on Numerical Fluid Mechanics* 27.

Hurle, D. T. J., Jakeman, E., Johnson, C.P. (1974) Convective temperature oscillations in molten gallium. *Journal of Fluid Mechanics* 64, 565-576.

Krane, R. J., Jessee, J. (1983) Some Detailed Field Measurements for a Natural Convection Flow in a Vertical Square Enclosure. *Proceedings Asme-Jsme Thermal Engineering Joint Conference 1: 323-329.*

Liu, J. P., Tao, W.Q. (1999) Bifurcation to oscillatory flow of the natural convection around a vertical channel in rectangular enclosure. *International Journal of Numerical Methods for Heat & Fluid Flow* 9, 170-185.

Metals Handbook (1990) Properties and Selection: Nonferrous Alloys and Special-Purpose Materials, *10th ed. 2. ASM International, Chicago 536-538*.

Pratte, J. M., Hart, J. E. (1990) Endwall driven, low Prandtl number convection in a shallow rectangular cavity. *Journal of Crystal Growth* 102, 54-68.

Roux, B, Bontoux, P, Henry, D. (1985) Numerical and theoretical study of different flow regimes occurring in horizontal fluid layers, differentially heated. In Macroscopic

Modelling of Turbulent Flows (ed. U. Frisch, J. B. Keller, G. Papanicolaou & O. Pironneau). *Lecture Notes in Physics* 230, 202-217.

Roux, B. (1990) GAMM Workshop: Numerical Simulation of Oscillatory Convection in low-Pr Fluids. *Notes on Numerical Fluid Mechanics* 27.

Semma, E., El Ganaoui, M., Bennacer, R., Chaddadi, A. (2004) Effects of the thermocapillary convection on the flow stability and the interaction with solid/liquid interface in directional solidification. *Mechanics & Industry* 5, 613-619.

Stevens, J. L., Lopez, J. M., Cantwell, B. J. (1999) Oscillatory flow states in an enclosed cylinder with a rotating endwall. *Journal of Fluid Mechanics* 389, 101-118.

Winters, K. H. (1988) Oscillatory convection in liquid metals in a horizontal temperature gradient. *International Journal for Numerical Methode in Engineering* 25, 401-414.

Zhao, Y., Lei, C., Patterson, J.C. (2016) Natural transition in natural convection boundary layers. *International Communications in Heat and Mass Transfer*76, 366-375.

Zhou, H., Zebib, A. (1992) Oscillatory Convection in Solidifying Pure Metals. *Numerical Heat Transfer, Part A* 22, 435-468.